Acta Acustica 2024, **8**, 20

https://doi.org/10.1051/aacus/2024012

Topical Issue - Virtual acoustics

Available online at:
https://acta-acustica.edpsciences.org

SCIENTIFIC ARTICLE OPEN ACCESS

The radiation from railway wheel modes and their effect on loudness, sharpness, and equivalent pressure level

Jannik Theyssen*

Chalmers University of Technology, Division of Applied Acoustics, Department of Architecture and Civil Engineering, Sven Hultins Gata 8a, 41258 Gothenburg, Sweden

Received 30 January 2024, Accepted 17 April 2024

Abstract – The noise of railway wheels is one of the main contributors to railway rolling noise. Auralization, the rendering of sound fields from virtual sources, is a promising tool for studying rolling noise, as it enables the study of perceptual qualities of noise. Generating such sound fields based on physical models requires knowledge of the structural vibrations and radiation characteristics of the wheels. The vibration and radiation of a railway wheel are typically dominated by highly undamped modes. The amplitudes of the various modes depend on the roughness excitation and the contact position of the wheel on the rail. For auralization, it is relevant to investigate which modes are significant in reproducing the equivalent sound pressure level (SPL), as well as psychoacoustic quantities. Identifying significant modes can also help simplify the physical model. This article explores the influence of lateral contact positions on wheel radiation and analyzes the modal contributions to pass-by SPLs. Using a timedomain prediction model for the sound pressure produced by one wheel as it passes a stationary track side position, the psychoacoustic quantities loudness and sharpness were investigated. The smallest number of modes required to reproduce equivalent pressure levels and psychoacoustic quantities is identified for two contact positions. For simplicity, the discussion is limited to one wheel, surface roughness, and vehicle speed. The results show possible simplifications in auralization models and can enable noise mitigation with a focus on psychoacoustic parameters.

Keywords: Railway rolling noise, Wheel modes, Psychoacoustics, Auralization

1 Introduction

Auralization describes the process of rendering a sound field from virtual sources [1]. Auralization of wheel/rail noise enables working with environmental noise problems in new ways compared to working with equivalent levels, opening up for investigating psychoacoustic metrics and more intuitive communication with a broader public. Addressing the human response can be especially relevant in the context of railway wheels, which produce a distinct piercing, metallic noise that may cause discomfort. The noise originates from the roughness-excited vibrations of the wheel, which is characterized by its strong modal behavior. A realistic auralization of wheel noise thus requires knowledge about the contributions of various modes to the pass-by noise signal.

The modes of the wheel are similar to those of a circular disc, which can be classified based on their number of nodal diameters (κ), their number of nodal circles (m) and their main direction of motion (axial, radial, or circumferential): (κ, m, a/r/c) [2]. During rolling on a straight track, the main direction of excitation at the wheel tread is radial. Since modes with strong axial motion on the wheel hub are comparatively good acoustic radiators, modes with a strong coupling between the radial direction at the tread to the axial direction on the hub are typically dominant noise sources [3]. The lateral excitation position of the wheel has therefore a large influence on the wheel radiation [4].

The auralization of wheel noise has been realized in different ways: The VAMPASS modeling tool developed in the SILENCE project [5] uses equivalent point sources for the wheels, where the TWINS model [6] provides the relevant sound power. Pieren et al. [7] use digital filters to model the mechanical behavior of the wheels and the radiation of the wheels. Similarly to engineering models such as CNOSSOS-EU [8], Pieren's model uses a transfer function from the wheel velocity at the wheel-rail contact point to the sound power. Maillard et al. [9, 10] calculate the axial velocity of the wheel by modal superposition of the wheel modes and then use a Rayleigh approximation to predict the sound power radiated by the wheel. To generate sound pressure signals from the moving wheel, it is then represented by an equivalent point source. The modeling approach in the SILVARSTAR project [11] also uses

*Corresponding author: jannik.theyssen@chalmers.se

equivalent point sources for the wheels distributed along the train. The sound power of each source is again evaluated using the TWINS model.

With the dominance of the wheel modes in the radiation, the question arises which of the modes are relevant contributors to the sound. This question is twofold, as the modal contributions can either be measured in terms of equivalent pass-by sound pressure level (SPL) or in terms of their effect on the perception. Previous work by the author [4] quantifies differences in the equivalent SPL during a pass-by when removing the sound pressure contribution from individual modes. However, this previous work does not address psychoacoustic quantities.

This article summarizes the algorithm that allows the prediction of the pass-by pressure signal produced by each mode of a passing wheel, as developed in [12]. The time-domain simulation of the rolling contact forces and the wheel modal amplitudes allows for predicting the sound pressure in a stationary track-side point based on the roughness excitation at the rolling contact point. Furthermore, the algorithm uses distinct, simulated directivities for each wheel mode. The sound pressure signals produced using this model are described in [4] and are further analyzed here in terms of their psychoacoustic effects. Specifically, the psychoacoustic quantities of loudness and sharpness are investigated. Loudness and sharpness are related to the perceived annoyance and, inversely, pleasantness [13]. These two psychoacoustic quantities are selected since their calculation from the time signals is straightforward. The analysis is limited to one wheel, vehicle speed, and combination of wheel and rail surface roughness; however, two lateral contact positions are discussed.

Section 2 describes the modeling approach, introduces the wheel and track geometry, and presents the properties of the contact. Section 3 reports and discusses the results of the simulations related to the wheel/rail contact forces, the pass-by sound pressure, and the implications for the auralization of the signal. Section 5 concludes the article.

2 Model description

The model used for the prediction of the sound radiation from railway wheels was developed in a recent doctoral thesis [12, 14], using previous work by Pieringer et al. [15] for the wheel/rail contact and interaction. The modeling approach consists of three main components, the wheel dynamics, the wheel-rail interaction, and the sound radiation, which are summarized below.

2.1 The wheel dynamics

The dynamic response of the wheel is modeled in a finite element approach, specifically the waveguide FE method for curved waveguides [16–18]. This method reduces the 3D domain formulation to multiple 2D problems by assuming a harmonic oscillation around the circumference of the wheel. A harmonic system of equations is then solved for each whole number of oscillations κ, also called the number of nodal diameters [3]. This produces the eigenfrequencies ω_l and the mode shapes $\mathbf{\Phi}_l$ of the wheel. The three-dimensional velocity vector v at position $\mathbf{g} = [g_\theta,\ g_y,\ g_r]^T$ on the wheel at angular frequency ω

$$\mathbf{v}(\mathbf{g},\omega) = \sum_l A_l(\omega)\mathbf{\Phi}_l(\mathbf{g}) \tag{1}$$

is obtained by modal superposition. The modal amplitude A_l is

$$A_l(\omega) = j\omega b_l \mathbf{F}_e(\omega)\mathbf{\Phi}_l(\mathbf{g}_c) \tag{2}$$

with the point force $\mathbf{F}_e(\omega) = [\mathbf{F}_\theta(\omega),\ F_y(\omega),\ F_r(\omega)]^T$ and the mode shape $\mathbf{\Phi}_l$ where $\mathbf{\Phi}_l(\mathbf{g}_c)$ is a three element vector that contains the deflection of mode l at the contact position of the wheel on the rail $\mathbf{g}_c$ in circumferential, axial, and radial direction. The term

$$b_l(\omega) = \left(\Lambda\left(\omega_l^2 - \omega^2 + 2j\omega\omega_l\zeta_l\right)\right)^{-1} \tag{3}$$

describes the vibrational decay in the structure with the modal damping coefficient ζ_l, which is 10^{-3} for $\kappa = 0$, 10^{-2} for $\kappa = 1$, and 10^{-4} for $\kappa < 2$ (cf. [3]), and the modal mass

$$\Lambda_l = \mathbf{\Phi}_l^T \mathbf{M} \mathbf{\Phi}_l \tag{4}$$

where $\mathbf{M}$ is the mass matrix from the WFE system of equations [19]. The prediction of the wheel structural response serves two purposes: one, the velocity field is input to the sound radiation module, and two, the receptance at the rolling point on the wheel is needed for the prediction of the wheel/rail interaction. From this receptance, displacement impulse response functions are calculated by inverse Fourier transform. The primary suspension and the rigid body modes of the wheelset are included in the wheel model to predict contact forces, as the wheel/rail interaction model would otherwise be too stiff [12].

For the wheel/rail interaction, a modal base of 560 modes is used, allowing for a high-frequency interaction at up to 28 kHz. However, for the sound radiation prediction only the 58 modes below 8 kHz are included for computational reasons and since modes above 8 kHz are less relevant due to the rolling contact filter [3].

In the following, half of the radial cross-section of a reprofiled wheel of type BA093 with a rolling radius of 0.469 m is used as the geometry. A detailed modal analysis of this wheel is carried out in [14, 18]. Half of the cross section is discretized into 146 quadrilateral 9-node elements as shown in Figure 1. Two of the nodes are used to investigate the effect of different lateral contact positions on the radiated sound pressure. These two nodes are located on the running surface, 6.4 cm and 9.4 cm in lateral direction from the flange back, respectively.

Figure 2 shows the corresponding point mobilities. Notice the large dynamic range due to the lightly damped modes. Changing the contact node can change the magnitude of the resonances and the location of the anti-resonances for some modes. This is due to the different radial deflection at the different nodes in each mode shape.

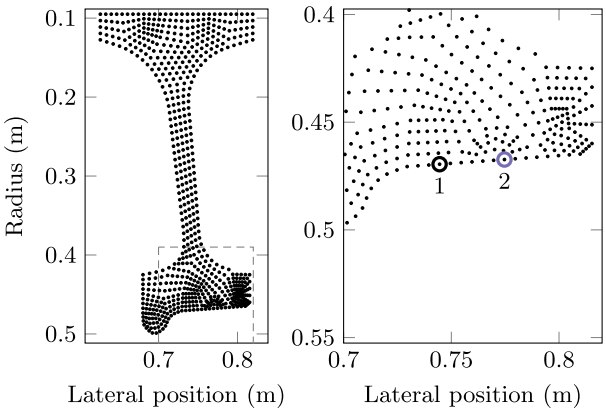

Figure 1. Wheel geometry, FE nodes (represented as dots) and the two excitation positions.

Figure 3 shows these radial deflections for the four modes highlighted in Figure 2. The resonance peak at the eigenfrequency of the first mode (4, 0, a) is small for excitation at Node 1 and increases for excitation at Node 2 due to the increasing radial response of the mode shape. Similar effects can be observed for the other modes and contact nodes.

2.2 The wheel/rail interaction

The interaction between the wheel and the track is calculated in the time domain using moving Green's functions [20, 21]. Green's functions for the wheel dynamic response are evaluated by inverse Fourier transform of the mobilities derived above. This time-domain approach allows for including non-linear effects in the contact patch. The contact area is discretized and, at each time step, Kalker's variational method [22] is used to solve the normal contact problem. A three-dimensional profile of the roughness of the wheel and rail is considered. The tangential wheel/rail interaction and contact can be included [21], but have been neglected here. The rotation of the wheel is neglected here. Including it would produce two peaks in the mobility of the wheel close to the eigenfrequency of each mode [3].

For this example, a pass-by with a vehicle speed of $v = 100$ km/h is simulated. A track consisting of rails with a UIC60 E2 profile on monobloc concrete sleepers in ballast is modeled with beam finite elements in DIFF [23]. This implies that the track response is identical even when changing the contact node on the wheel. The track parameters are listed in [24]. The rail surface roughness used in the simulation was measured on a high-speed line in Germany [25]. A surface roughness measurement on a wheel with composite brake blocks [26] serves as input to the wheel model. Average spectra of the roughness of the wheels and rails are shown in Figure 4, with the upper limit for the track roughness in acoustic measurements defined in ISO 3095 [27] for reference.

2.3 The sound radiation

The Fourier series Boundary Element method (FBEM) [18, 28] is used to calculate the sound radiated by each wheel mode l, with unit modal amplitude, for a stationary wheel. The sound pressure is evaluated on a sphere with a 5 m radius around the wheel center. In a second step, the sound field of each mode is decomposed into spherical harmonic (SH) equivalent source components [12]. This has the advantage that sound pressure transfer functions $H_l(\Delta\mathbf{x},\ \omega)$, $[H_l(\Delta\mathbf{x},\ \omega)]$ = Pa / (m/s), can be efficiently calculated for any receiver position in 3D space [14]. The vector $\mathbf{x}$ here describes the positions of the source and receiver, where $\Delta\mathbf{x} = \mathbf{x}_\mathrm{R} - \mathbf{x}_\mathrm{S}$ with the location of the receiver $\mathbf{x}_\mathrm{R} = [0,\ y_\mathrm{R},\ z_\mathrm{R}]^T$ and the location of the source $\mathbf{x}_\mathrm{S} = [x_\mathrm{S},\ y_\mathrm{S},\ z_\mathrm{S}]^T$. These transfer functions describe the sound pressure at a receiver point produced by the wheel mode l with a unit modal amplitude. During the simulation of the rolling of the wheel on the rail, this modal amplitude varies due to the vibrational decay in the wheel and the varying modal excitation. The decay corresponding to the term $b_l(\omega)$ in equation (3) can be expressed analytically in the time domain,

$$b_l(t) = \frac{e^{-2\omega_l\zeta_l t}}{\Lambda_l\omega_l'}\sin\left(\omega_l' t\right)H(t) \quad \text{with}\ \omega_l'\omega_l\sqrt{1-\zeta_l^2} \tag{5}$$

with ω_l, the eigenfrequency of mode l, H(t), the Heaviside function. It has the unit $[b_l]$ = m/(Ns). The modal excitation becomes

$$F_{A,l}(t) = \frac{d}{dt}\mathbf{F}_e(t)\mathbf{\Phi}_l(\mathbf{g}_\mathrm{c}) \tag{6}$$

with the unit $[F_{A,l}(t)]$ = N/s when expressed in the time domain. The convolution of $b_l(t)$ and $\mathrm{F}_{A,l}(t)$ produces a time domain expression for the modal amplitude in equation (2),

$$q_{S,l}(t) = \int_{-\infty}^{t} F_{A,l}(t)b_l(t-\tau)d\tau, \tag{7}$$

of unit $[q_{S,l}(t)]$ = m/s which describes the amplification of each mode at each time step, taking into account the history of all contact forces and the dynamic response of the mode. The inverse Fourier transform of $H_l(\Delta\mathbf{x},\ \omega)$ produces impulse response functions $h_l(\Delta\mathbf{x},\ t)$ of unit $[h_l(\Delta\mathbf{x},\ t)]$ = Pa/m of the pressure signal due to unit modal excitation. The convolution of $q_{\mathrm{S,l}}$ and h_l then allows for calculating the pass-by pressure at a stationary receiver position of mode I

$$p_\mathrm{l}(0,\ y_\mathrm{R}, z_\mathrm{R}, t) = \int_{-\infty}^{t} q_{\mathrm{S,l}}(\tau)h_\mathrm{l}(v\tau, t-\tau)d\tau, \tag{8}$$

where the source location and time are linked by the wheel velocity v, $t = x_\mathrm{S}/v$. The computational advantage of this modal approach is that the acoustic propagation functions $H_l(\omega)$ are rather smooth, so they can be evaluated with a broad frequency spacing in the Boundary Element solution. The total pressure is then calculated as the sum of all modal contributions,

$$p_\mathrm{l}(0,\ y_\mathrm{R}, z_\mathrm{R}, t) = \sum_l p_\mathrm{l}(0,\ y_\mathrm{R}, z_\mathrm{R}, t). \tag{9}$$

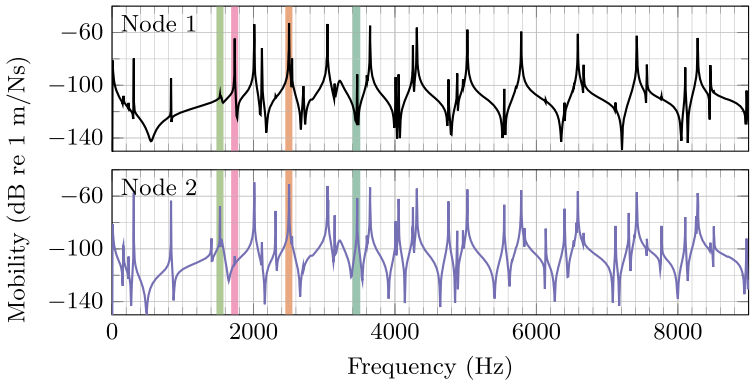

Figure 2. Predicted radial point mobility at each contact point. The four highlighted resonances belong to the modes (4, 0, a), (2, 1, a), (3, 0, r), and (3, 2, a), sorted by increasing frequency.

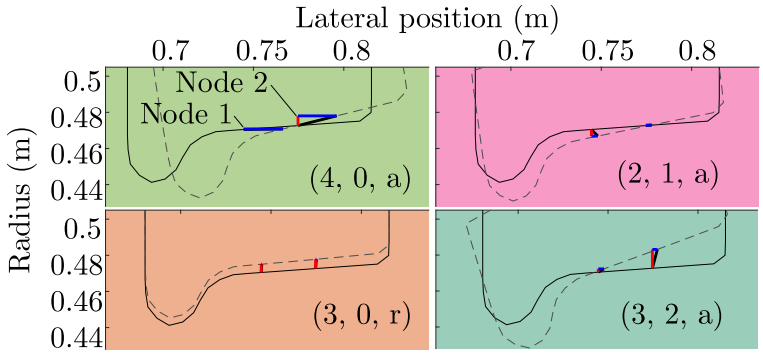

Figure 3. Wheel tread motion at four eigenmodes. The radial and axial displacement at the four excitation nodes are indicated with red and blue lines, respectively.

As all modes contribute to the surface velocity of the wheel, the contributions from individual modes are correlated and derived quantities as, e.g., the equivalent SPL can not be evaluated for each mode individually.

3 Rolling contact forces, pressure signals and psychoacoustic parameters

This section first shows the effect of the different excitation positions on the rolling contact force and on the radiated sound. These differences are due to the varying excitation of the modes. It is then explored which subset of modes is relevant for reproducing the equivalent SPL and psychoacoustic quantities during the pass-by.

3.1 Differences in the rolling contact force

The wheel/rail interaction is influenced by the lateral contact position. The large mobility at wheel resonances typically leads to a reduced rolling contact force at this frequency (similar to the low force needed to deflect a soft spring). Analogously, large rolling contact forces are expected at the anti-resonances. This is visible in the spectrum of the rolling contact forces around the mode (3, 2, a) in Figure 5, where the dip at 3460 Hz marks the resonance,

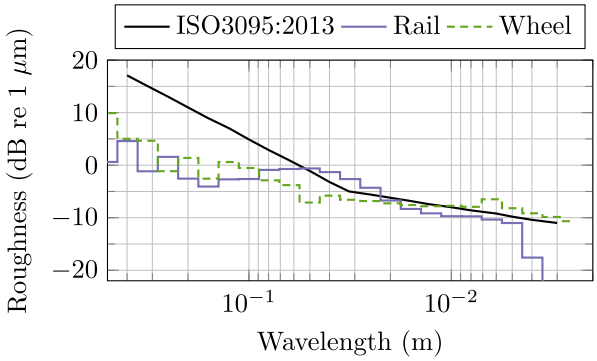

Figure 4. Average wheel and rail roughness spectra, in one-third octave bands.

while the frequency of the anti-resonance changes with the excitation position.

Figure 6 presents the frequency spectrum of the rolling contact force for excitation position at Node 1 (see Fig. 1). Sharp dips mark the resonance frequencies of modes with high radial mobility at the contact point. The rolling contact force spectra for Node 2 are are presented as relative differences to the those of Node 1. Large differences of up to 20 dB are observable for specific modes, many of

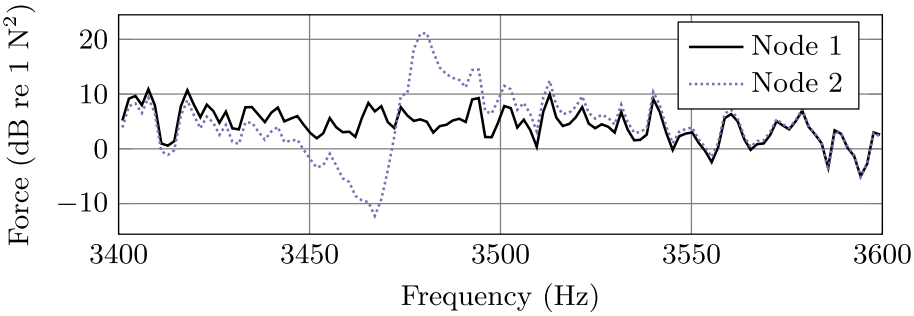

Figure 5. Effect of moving the lateral wheel-rail contact position on the rolling contact force power spectrum around the mode (3, 2, a).

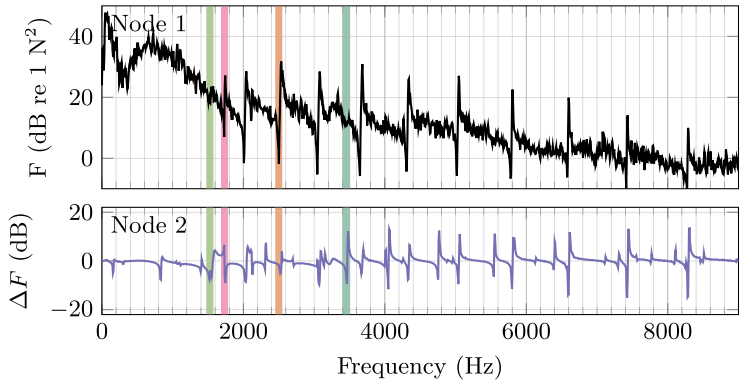

Figure 6. Power spectrum of the rolling contact forces for Node 1, and the spectra for Node 2 normalized with Node 1. Modes highlighted as in Figure 2.

which are axial modes. One such example is the mode (3, 2, a), which is more efficiently excited due to its increasing radial component towards the outer excitation positions. The four highlighted regions mark the location of the modes described above.

3.2 Contact point and pass-by pressure

The pass-by pressure is evaluated for each mode at a standard receiver position at $y = 7.5$ m distance from the track center and $z = 1.2$ m above the rail. An increase of 6 dB in the SPL, evaluated by taking the root-mean-square value of the generated signal, is observed when changing the excitation position from Node 1 to Node 2 (60.6 dB to 66.7 dB, not A-weighted). A possible reason for this large increase could be the neglected lateral interaction at the contact point, which leads to an overestimation of the contribution of the axial modes [3, 29]. Audio examples of the sound pressure signals for the various excitation positions are available online [30]. Figure 7 shows the SPL of excitation Node 2 relative to Node 1 in one-third octave bands. In general, the outer excitation position corresponds to higher levels.

To analyze the differences in the third-octave bands, the modal contributions to the total sound radiation are investigated. An equivalent SPL $L_{\mathrm{p,eq,1s}}$ of each mode during one second of the pass-by, centered around the pass-by instant, is calculated. With one second corresponding to approximative 28 m traveling distance at the chosen speed of 100 km/h, the pressure level is averaged for wheel positions between about $x = -14$ m to 14 m. The $L_{\mathrm{p,eq,1s}}$, is of each wheel mode is compared for the two excitation nodes in Figure 8 which shows the difference in level between an excitation at Node 1 and Node 2. The modes are arranged in the dispersion diagram of the wheel [14, 18], where the different types of modes are indicated by marker shapes. Modes connected by dashed lines share the same number of nodal circles. The largest increase is observable for axial modes,

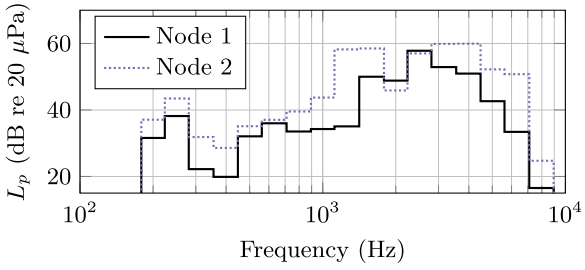

Figure 7. Total SPL for the two excitation positions.

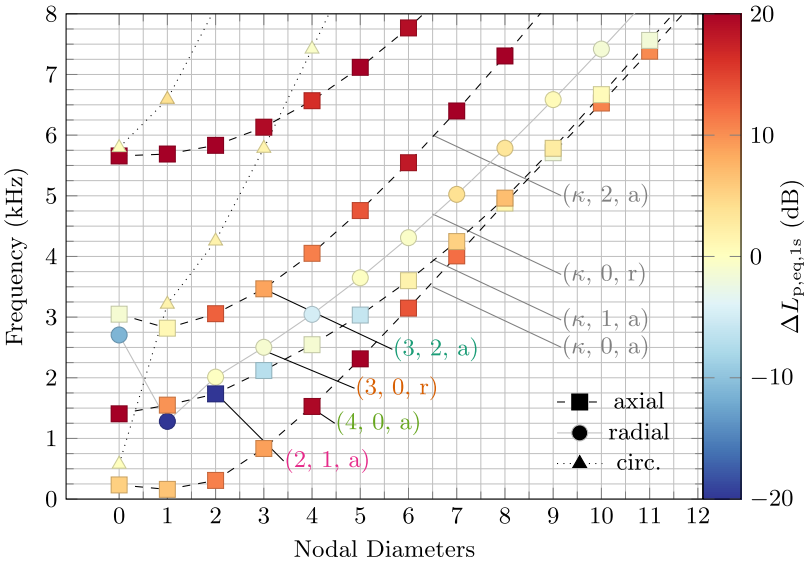

Figure 8. Dispersion diagram where each marker represents a mode of the wheel. The color indicates the difference in $L_{\mathrm{p,eq,1s}}$ is between excitation at Node 1 and Node 2, where positive differences correspond to larger radiation for an excitation at Node 2.

specifically axial modes with two and three nodal circles above about 5 kHz and the modes (4, 0, a), (5, 0, a), and (0, 1, a). The largest decrease is observed for the radial mode (1, 0, r) and the axial mode (2, 1, a). These differences are to a large extent explained by the difference in the point mobilities at the two excitation node positions.

However, a large increase in the equivalent pressure level does not necessarily mean that a mode is more relevant to the absolute sound pressure at a stationary receiver position. Quantifying this relevance is explored in the following subsection.

3.3 Modal contribution to the pass-by sound pressure and psychoacoustic quantities

Since the various modes contribute to the pass-by pressure level to varying degrees, their relative significance should be quantifiable in a ranking. Identifying modes significant to the equivalent SPL can be relevant for, e.g., designing noise mitigation measures such as tuned wheel dampers, or identifying relevant modes for an auralization. In the following, this relative significance is evaluated for three quantities: the equivalent pass-by pressure level, the estimated loudness, and the estimated sharpness of the signal. Since the sound pressure signals produced by the modes are correlated at the receiver point, it is not possible to directly compare their relative contributions. Instead, modal contributions to the pass-by pressure are removed iteratively from the total sound pressure to quantify their significance. Note that only the radiation and not the dynamic behavior of the wheel is altered here, as if introducing a perfect acoustic absorber that only absorbs the radiation from a single mode.

The pressure signals produced by the individual modes are iteratively removed from the total according to the following algorithm: First, a reference level L_0 at the stationary receiver position is calculated. This reference level includes all modes. Then, the mode with the least significant contribution to this reference level is determined by iteratively removing each mode and evaluating the level differences to the reference level. This mode is removed and a new temporary reference level L^- is calculated by summation of the remaining modal contributions. Iteration through all modes leads to a ranking of modes from least to most significant. This procedure is repeated for the total SPL, the psychoacoustic loudness, and the psychoacoustic sharpness. The loudness is evaluated according to the ISO standard 532-1 [31], for free field conditions, with the method for stationary sounds. The sharpness is evaluated according to the DIN 45692 [32] standard.

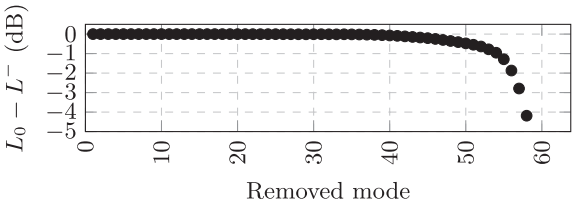

Figure 9. Iterative removal of modal contribution to the total sound pressure: pressure level difference of the remaining modes L^- compared to the initial pressure level L_0.

Figure 9 shows the level differences between the level L^- and the initial pressure level L_0. Removing 50 of the 58 modes considered produces a signal that is within 0.5 dB of the reference level, independent of the excitation position. Figure 10 shows the highlighted section in Figure 9 and indicates the removed modes. In both cases, only six modes produce an equivalent SPL within 1 dB of the reference level L_0. However, the sets of six modes are not identical for both excitation positions. Only the modes (3, 2, a), (4, 1, a) and (4, 2, a) are found in both sets.

Producing a signal with a similar equivalent SPL does not necessarily translate into a realistic auralization.

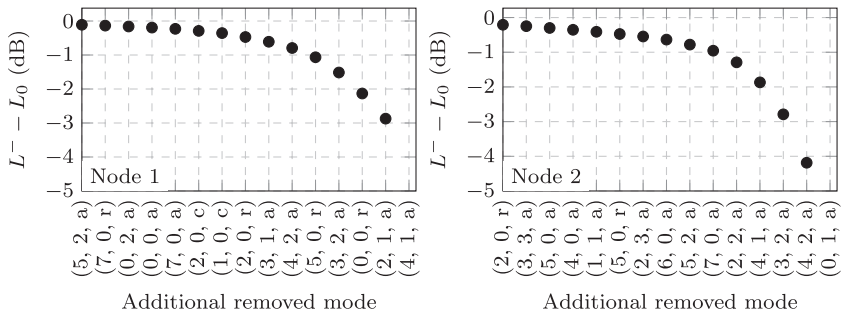

Figure 10. Section of Figure 9. Significant modes based on the equivalent pass-by SPL criterion.

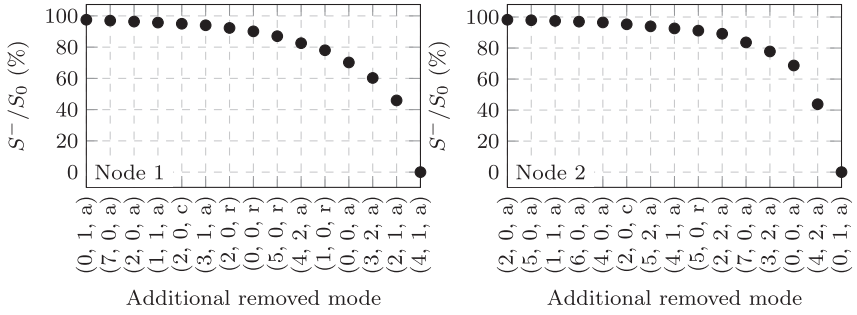

Figure 11. Significant modes based on the psychoacoustic loudness criterion.

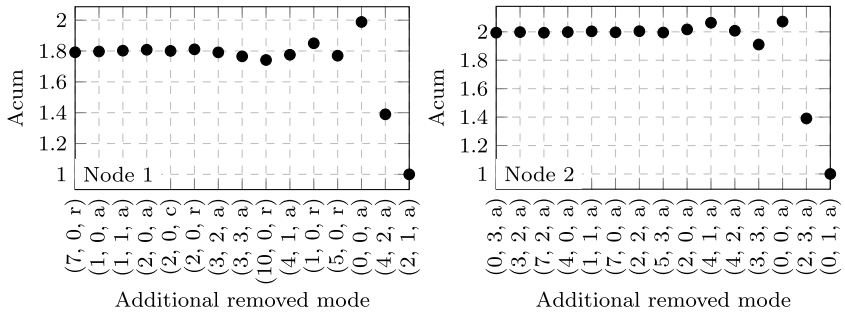

Figure 12. Significant modes based on the psychoacoustic sharpness criterion.

The above analysis is repeated with the criterion of minimizing the change in psychoacoustic loudness in each iteration. Including all modes produces a reference loudness S_0 of about 19.6 sone (excitation at Node 1). Figure 11 shows the difference in estimated loudness for the final 15 iterations, compared to the reference level S_0, for both excitation positions. To achieve a signal that is perceptually at least 95% as loud as So, a set of at least ten modes is required for both excitation positions (90% – seven modes, 99% – 19 modes). There is an overlap of five modes between the 95%-set and the one for the equivalent pressure level, including the modes (4, 1, a), (3, 2, a), (0, 0, a), (4, 2, a) and (5, 0, r).

Finally, the modes are ranked according to their influence on estimated sharpness in the same way. The sharpness varies in the positive and negative directions during iteration, as shown in Figure 12. This variation is expected as the sharpness describes a ratio between the high-frequency content to the overall level. Removing a mode with a low eigenfrequency, such as the mode (0, 0, a), leads to a significant change of this ratio towards higher sharpness. The outer excitation position at Node 2 leads to a higher total sharpness, likely due to the increased excitation of the high frequency modes (2, 3, a) and (3, 3, a). The sharpness is evaluated by employing a simple weighting function to emphasise the spectral components above about 2.9 kHz. As a consequence, the modes relevant for the psychoacoustic sharpness are, to a large degree, a subset of the modes relevant for the psychoacoustic loudness. Further, especially modes with the lowest and highest eigenfrequencies are relevant. With about four modes, a similar sharpness is achieved as with all modes included. Only the mode (0, 0, a) is present in the sets for Node 1 and Node 2.

These results are summarized in Figure 13. In these dispersion diagrams (cf. Fig. 8), each marker represents one

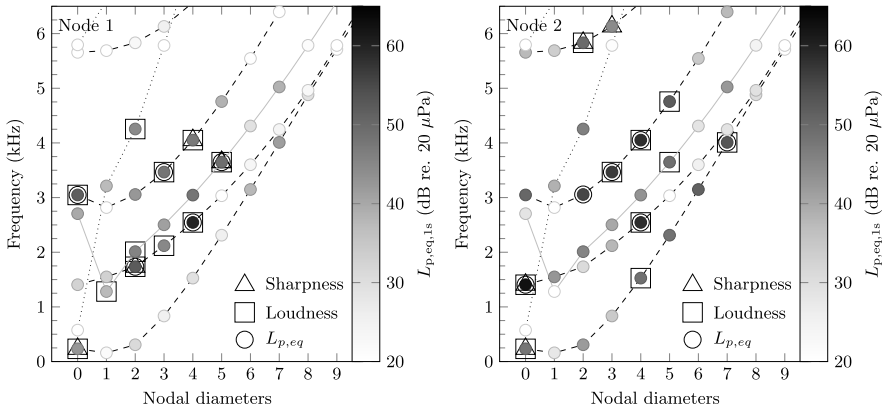

Figure 13. Set of significant modes for the three analyzed criteria: sharpness, loudness, and equivalent pass-by pressure level (L_p), indicated by triangular, square and round markers. The color scale corresponds to the 1 s equivalent SPL.

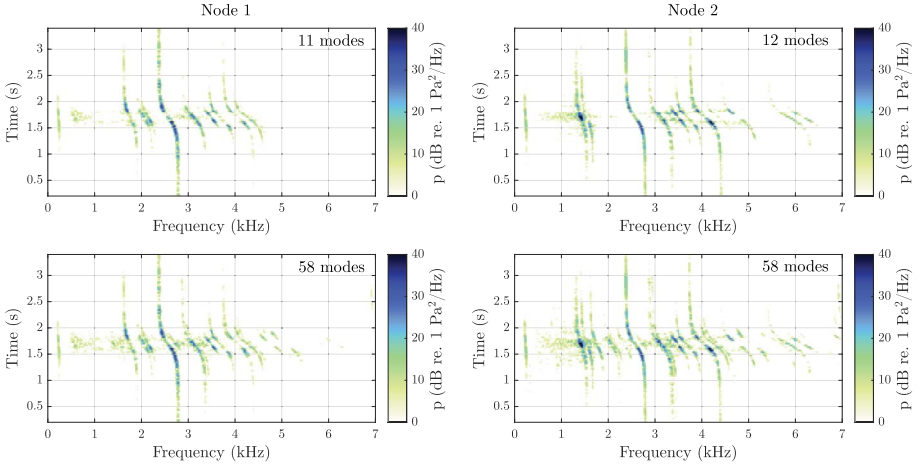

Figure 14. Power spectral density spectrograms of the pass-by sound pressure for excitation at Node 1 and 2 (left and right, respectively) including all 58 modes and the selected 11 modes.

mode and the saturation of each marker indicates the corresponding equivalent pressure level. The sets of relevant modes identified in the analysis above are indicated by triangular, square, and circular markers. Figure 13 shows that modes relevant for the psychoacoustic sharpness are a subset of the modes relevant for the equivalent pass-by sound pressure and the loudness. The set of modes relevant for the loudness includes most modes relevant for the equivalent pass-by pressure level, with the exception of the mode (2, 2, a) for an excitation at Node 2. In general, radial and axial modes with one and two nodal circles are the most relevant modes for the equivalent SPL. This is in line with previous literature [3]. Including these modes up to order 5, and adding the mode (0, 0, a), covers the relevant modes for the psychoacoustic loudness for the central excitation at Node 1. The off-center excitation at Node 2 leads to higher contributions from axial modes with zero nodal circles, which also contribute to the loudness.

To summarize, it is found that for the presented pass-by prediction, a set of 11 modes seems sufficient to reproduce the researched psychoacoustic quantities. The pass-by pressure produced by all 58 included modes is compared to the selected subsets as spectrograms in Figure 14. The doppler shift is clearly visible as the spectrum is dominated by narrow peaks near the eigenfrequencies. Considering the relatively large displayed dynamic range of 40 dB and the significant reduction of modes, the spectrograms are quite similar.

4. Discussion

This study presents results for two pass-by simulations in which only the lateral contact position of the wheel is changed. Results such as the significant modes are certainly influenced by the chosen parameters for these simulations such as the wheel and rail roughness and dynamic properties, the applied modal damping values, the wheel radiation efficiency, the vehicle speed and preload. Since the sets of significant modes are rather small, it could be convenient to limit the calculation to these modes in an auralization. However, with the limitation laid out above, it is advisable to generally include at least the axial modes with one and two nodal diameters, and radial modes with one nodal

diameter, up to the frequency where the rolling contact filter is relevant. In addition to that, the mode (0, 0, a) and possibly the first few axial modes with zero nodal diameters should be included. Axial modes with three nodal diameters that are significantly excited should be included as well as they contribute to the perceived sharpness.

The researched psychoacoustic quantities do not include a time structure and are therefore not sufficient for indicating a realistic representation of a real pass-by signal, i.e., one could produce sound signals with identical values for loudness and sharpness that have otherwise little resemblance to that of a passing railway wheel.

Listening experiments would be necessary to quantify how realistic the produced signals are, and (b) at what point the reduction of modes creates audible differences. Subjective assessments of the resulting sounds are not carried out, however, by listening to the version with 11 and 12 modes, respectively, and comparing to the version with 58 modes, the author is certain that most people are able to distinguish the two in a direct comparison. Audio examples of the passby with all modes and with a reduced number of modes are provided online [33]. These researched quantifiers can, however, suffice for an estimation of the annoyance.

5 Conclusions

A time-domain model for predicting pass-by rolling noise from railway wheels is presented. The modeling approach uses Finite Element and Boundary Element methods to predict the modes of the wheel and the radiation from each mode. The sound field produced by each mode, with unit modal amplitude, is represented in a spherical harmonic formulation, which facilitates the calculation of acoustic impulse responses describing the pressure response at a track side position for any position of the wheel. By describing the modal amplitude in the time domain, an efficient prediction of the pass-by pressure signal is achieved.

This paper investigates the influence of the wheel's lateral contact position in two different positions. Large differences in the contact force are observed for different contact positions. These differences are explained by the modal behavior of the wheel, which affects the relevant point mobility, leading to dips and peaks in the contact force spectrum at resonances and anti-resonances, respectively. An increase of up to 6 dB is observed in the equivalent SPL between the lateral contact positions. A possible explanation is that the lateral interaction was neglected in the rolling contact, which can lead to an overestimation of the contribution of the axial modes. Comparison of the frequency spectra of the equivalent SPL showed the highest overall levels for the excitation position farther away from the flange. Also the psychoacoustic sharpness is higher for this excitation position. The increase is different across the frequency spectrum depending on the level of excitation of each mode. Analyzing the contribution of each mode to the pass-by pressure shows a strong dependence on the contact position.

It is observed that only contributions from a few modes, here 4–6, are needed to predict the SPL to within 1 dB error. However, the set of modes significant for the SPL varies between lateral positions. Sets of significant modes are also identified for the psychoacoustic quantities loudness and sharpness. The set of modes relevant for reproducing the loudness generally includes the set relevant for the equivalent SPL; however, it is larger (here 11–12 modes). Clearly, the low-frequency mode (0, 0, a) is relevant for the loudness but not for the equivalent SPL. Modes relevant for reproducing the psychoacoustic sharpness are generally also relevant for the perceived loudness and found at the low and high ends of the frequency spectrum. Here, including the sound radiation of only four modes produces a signal with a sharpness similar to that when all modes are included in the prediction.

Future studies could include the vertical/lateral coupling in the contact point, various vehicle speeds and roughness excitations and the rotation of the wheel.

Acknowledgments

The current study is part of the ongoing activities in CHARMEC – Chalmers Railway Mechanics (www.charmec.chalmers.se).

Funding

Parts of the study have been funded from the European Union's Horizon 2020 research and innovation programme in the In2Track3 project under grant agreements No. 101012456.

Conflicts of Interest

The Author declares no conflict of interests.

Data availability statement

Research data associated with this article are available on request.

References

1. M. Kleiner, B-I, Dalenbäck, P. Svensson: Auralization – an overview. Journal of the Audio Engineering Society 41, 11 (1993) 861–875. https://www.aes.org/e-lib/browse.cfm?elib=6976.
2. D. Thompson, C. Jones: Sound radiation from a vibrating railway wheel. Journal of Sound Vibration 253, 2 (2002) 401–419.
3. D.J. Thompson: Railway noise and vibration: mechanisms, modelling and means of control, 1st edn. Elsevier, Amsterdam, Boston, 2009.
4. J. Theyssen, A. Pieringer: Towards auralization of pass-by noise from railway wheels: sensitivity of the lateral contact position, in Proceedings of the 10th Convention of the European Acoustics Association (Forum Acusticum), 2023, pp. 5621–5628.
5. E. Bongini, S. Molla, P.E. Gautier, D. Habault, P.O. Mattéi, F. Poisson: Synthesis of noise of operating vehicles: development within SILENCE of a tool with listening features, in B. Schulte-Werning, D. Thompson, P.-E. Gautier, C. Hanson, B. Hemsworth, J. Nelson, T. Maeda, P. de Vos, Eds., Noise and vibration mitigation for rail transportation systems, Notes on numerical fluid mechanics and multidisciplinary design. Springer, Berlin, Heidelberg, 2008, pp. 320–326.
6. D. Thompson, B. Hemsworth, N. Vincent: Experimental validation of the twins prediction program for rolling noise, part 1: Description of the model and method. Journal of Sound and Vibration 193, 1 (1996) 123–135.
7. R. Pieren, K. Heutschi, J.M. Wunderli, M. Snellen, D.G. Simons: Auralization of railway noise: Emission synthesis of rolling and impact noise. Applied Acoustics 127 (2017) 34–45.

8. The European Commission: COMMISSION DIRECTIVE (EU) 2015/ 996 – of 19 May 2015 – establishing common noise assessment methods according to Directive 2002/49/EC of the European Parliament and of the Council. Official Journal of the European Union L 168, 1 (2015) 1–823.
9. A. Kacem, J. Maillard, N. Martin, B. Faure: Caractérisation et auralisation de la contribution du rail dans le bruit ferroviaire, in: 14ème Congrès Français d'Acoustique, Le Havre, France, 23–27 Avril, 2018.
10. J. Maillard, A. Kacem, N. Martin, B. Faure: Physically-based auralization of railway rolling noise, in: Proceedings of the 23rd International Congress on Acoustics, Deutsche Gesellschaft für Akustik e.V. (DEGA), Aachen, 2019, pp. 1667–1674.
11. R. Pieren, F. Georgiou, G. Squicciarini, K. Heutschi, D. Thompson: VR demonstration of railway noise mitigation using auralised train pass-bys, in: Proceedings of the 10th Convention of the European Acoustics Association Forum Acusticum 2023, European Acoustics Association, Turin, Italy, 2024, pp. 5629–5635.
12. J. Theyssen, T. Deppisch, A. Pieringer, W. Kropp: On the efficient simulation of pass-by noise signals from railway wheels. Journal of Sound and Vibration 564 (2023) 117889.
13. H. Fastl, E. Zwicker: Psychoacoustics: facts and models. Springer Berlin Heidelberg, Berlin, Heidelberg, 2007.
14. J. Theyssen: Simulating rolling noise on ballasted and slab tracks: vibration, radiation, and pass-by signals. Doctoral Thesis. Chalmers University of Technology, Gothenburg, Sweden, 2022.
15. A. Pieringer, W. Kropp, D.J. Thompson: Investigation of the dynamic contact filter effect in vertical wheel/rail interaction using a 2D and a 3D non-Hertzian contact model. Wear 271, 1 (2011) 328–338.
16. S. Finnveden, M. Fraggstedt: Waveguide finite elements for curved structures. Journal of Sound Vibration 312, 4–5 (2008) 644–671.
17. P. Sabiniarz, W. Kropp: A waveguide finite element aided analysis of the wave field on a stationary tyre, not in contact with the ground. Journal of Sound Vibration 329, 15 (2010) 3041–3064.
18. F. Fabre, J.S. Theyssen, A. Pieringer, W. Kropp: Sound radiation from railway wheels including ground reflections: a half-space formulation for the fourier boundary element method. Journal of Sound Vibration 493 (2021) 115822.
19. C.-M. Nilsson, C. Jones, D. Thompson, J. Ryue: A waveguide finite element and boundary element approach to calculating the sound radiated by railway and tram rails. Journal of Sound Vibration 321, 3–5 (2009) 813–836.
20. A. Pieringer: Time-domain modelling of high-frequency wheel/rail interaction. Doctoral Thesis. Chalmers University of Technology, Gothenburg, Sweden, 2011.
21. A. Pieringer, W. Kropp, J.C.O. Nielsen: The influence of contact modelling on simulated wheel/rail interaction due to wheel flats. Wear 314, 1 (2014) 273–281.
22. J.J. Kalker: Three-dimensional elastic bodies in rolling contact, vol. 2 of solid mechanics and its applications. Springer, Netherlands, Dordrecht, 1990.
23. J. Nielsen, A. Igeland: Vertical dynamic interaction between train and track influence of wheel and track imperfections. Journal of Sound Vibration 187, 5 (1995) 825–839.
24. A. Pieringer, W. Kropp: Model-based estimation of rail roughness from axle box acceleration. Applied Acoustics 193 (2022) 108760.
25. D. Thompson, G. Squicciarini, J. Zhang, I. Lopez Arteaga, E. Zea, M. Dittrich, E. Jansen, K. Arcas, E. Cierco, F.X. Magrans, A. Malkoun, E. Iturritxa, A. Guiral, M. Stangl, G. Schleinzer, B. Martin Lopez, C. Chaufour, J. Wandell: Assessment of measurement-based methods for separating wheel and track contributions to railway rolling noise. Applied Acoustics 140 (2018) 48–62.
26. V. Delavaud: Modelisation temporelle de l'interaction roue/rail pour une application au bruit de roulement ferroviaire, Doctoral Thesis. ENSTA ParisTech, 2011.
27. ISO 3095:2013(E): Acoustics – Railway applications – Measurement of noise emitted by railbound vehicles, International Organization for Standardization, 2013.
28. A.H.W.M. Kuijpers, G. Verbeek, J.W. Verheij: An improved acoustic Fourier boundary element method formulation using fast Fourier transform integration. Journal of the Acoustical Society of America 102, 3 (1997) 1394–1401.
29. G. Cheng, Y. He, J. Han, X. Sheng, D. Thompson: An investigation into the effects of modelling assumptions on sound power radiated from a high-speed train wheelset. Journal of Sound Vibration 495 (2021) 115910.
30. J. Theyssen: Complementary files to the publication "Towards auralization of pass-by noise from railway wheels: sensitivity of the lateral contact position". Available at http://www.ta.chalmers.se/research/vibroacoustic-group/audio-examples/fa2023a/.
31. ISO 532–1:2017(E): Acoustics – Methods for calculating loudness – Part 1: Zwicker Method, International Organization for Standardization, 2017.
32. DIN 45692: Messtechnische Simulation der Hörempfindung Schärfe [Measurement technique for the simulation of the auditory sensation of sharpness], German Institute for Standardization, 2009.
33. J. Theyssen: Complementary files to the publication "The radiation from railway wheel modes and their effect on loudness, sharpness, and equivalent pressure level". Available at http://www.ta.chalmers.se/research/vibroacoustic-group/audio-examples/aa-2024a/.

Cite this article as: Theyssen J. 2024. The radiation from railway wheel modes and their effect on loudness, sharpness, and equivalent pressure level. Acta Acustica, **8**, 20.